High-Frequency Gravity Waves and Kelvin-Helmholtz Billows in the Tropical UTLS, as Seen From Radar Observations of Vertical Wind

Ajil Kottayil, Aurélien Podglajen, Bernard Legras, Rachel Atlas, Prajwal K, K. Satheesan, Abhilash S

Geophysical Research Letters

RESEARCH LETTER
10.1029/2024GL110366

High-Frequency Gravity Waves and Kelvin-Helmholtz Billows in the Tropical UTLS, as Seen From Radar Observations of Vertical Wind

Ajil Kottayil[1], Aurélien Podglajen[2], Bernard Legras[2], Rachel Atlas[2], Prajwal K[1], K. Satheesan[1,3], and Abhilash S[1,3]

[1]Satellite Remote Sensing and Applications, Advanced Centre for Atmospheric Radar Research, Cochin University of Science and Technology, Kochi, India, [2]Laboratoire de Météorologie Dynamique, IPSL, CNRS, ENS-PSL/Ecole Polytechnique/Sorbonne Université, Paris, France, [3]Department of Atmospheric Sciences, Cochin University of Science and Technology, Kochi, India

Abstract The present study analyzes novel observations of vertical wind (w) in the tropical upper troposphere-lower stratosphere obtained from a radar wind profiler in Cochin, India. Between December 2022 and April 2023, 63 consecutive 4 hr curtains of w were measured with a vertical spacing of 180 m and a sampling time step of 44 s, thus resolving almost the whole spectrum of vertical motions. Spectra of w strongly vary with altitude. They are generally flat up to the local Brunt-Väisälä frequency (BVF), but sometimes exhibit a peak of w variance closer to BVF, a feature which may be attributed to trapped gravity waves. At other times and locations, the w profiles reveal Kelvin-Helmholtz billows. Finally, the variability of w variance over the 4 month campaign period is investigated. Using brightness temperature from geostationary satellites as a convective proxy, it is found that w variance is highly correlated with fluctuations in convective activity.

Plain Language Summary Vertical wind is a key meteorological parameter. In the tropical Upper Troposphere Lower Stratosphere (UTLS, the atmospheric layer between 14 and 20 km altitude above sea level), it crucially affects the formation of clouds and the transport of trace gases, such as water vapor, ozone and radiatively active constituents. The ensuing impacts on stratospheric composition and the Earth radiative budget have consequences for surface weather and climate. However, only a few instruments are capable of measuring vertical wind accurately in clear air, and these include VHF radars. In this study, we analyze radar measurements of UTLS vertical wind over Cochin, India taken at a 44 s sampling rate and with a vertical resolution of 180 m. Thanks to its high quality and temporal resolution, the data resolves the full spectrum of vertical motions and provides invaluable insights into the complex dynamics of the UTLS. In particular, it suggests a frequent occurrence of trapped gravity waves in this region. Trapped waves are confined vertically due to a specific vertical structure of wind and stability, but propagate long distances horizontally. The study also finds a clear relationship between vertical wind magnitude in the UTLS and convective clouds in the troposphere.

Ajil Kottayil and Aurélien Podglajen contributed equally to the study.

Key Points:

- Measurements of the vertical wind throughout the upper troposphere and lower stratosphere (UTLS) from a recently built radar
- Observations of Kelvin-Helmholtz billows and trapped gravity waves in the tropical UTLS
- Impact of convection on clear-sky vertical wind variance in the tropical UTLS

Supporting Information:

Supporting Information may be found in the online version of this article.

Correspondence to:

A. Podglajen,
aurelien.podglajen@sorbonne-universite.fr

Citation:

Kottayil, A., Podglajen, A., Legras, B., Atlas, R., K, P., Satheesan, K., & S, A. (2024). High-frequency gravity waves and Kelvin-Helmholtz billows in the tropical UTLS, as seen from radar observations of vertical wind. *Geophysical Research Letters*, *51*, e2024GL110366. https://doi.org/10.1029/2024GL110366

Received 18 MAY 2024
Accepted 28 AUG 2024

1. Introduction

Vertical wind (w) is an important meteorological parameter determining the day-to-day weather development. In the tropical Upper Troposphere-Lower Stratosphere (UTLS), w mostly bears the signatures of small-scale phenomena: atmospheric convection (e.g., Dauhut et al., 2018; Grant et al., 2022; Schumacher et al., 2015), turbulence and dynamic instabilities (e.g., Fujiwara et al., 2003; Gisinger et al., 2020; Pfister et al., 1986; Podglajen et al., 2017), and gravity waves (e.g., Atlas & Bretherton, 2023; Wang et al., 2006). It impacts transport of trace species (Legras & Bucci, 2020; Sivan et al., 2022) and microphysical processes (e.g., Dinh et al., 2016; Jensen et al., 2016). The fine scales of the dynamical processes involved in w variability render its numerical modeling difficult (Atlas & Bretherton, 2023; Köhler et al., 2023) and resolution-sensitive. This means that atmospheric (re)analyses are poorly suited to study this parameter (Podglajen et al., 2020; Uma et al., 2021). On the observational side, only a handful of platforms have the ability to measure vertical wind in situ with sufficient resolution: research aircraft (e.g., Bacmeister et al., 1996; Schumann, 2019; Scott et al., 1990) and balloons (Hertzog & Vial, 2001; Podglajen et al., 2016). Alternately, w can be retrieved through active remote-sensing, including Doppler lidar and radar wind profilers.

Among very high frequency (VHF) radar facilities able to measure in the UTLS, only a few are located within the tropical belt. These data have nevertheless been instrumental in documenting the variability of w at low latitudes. In particular, the Indian MST (Mesosphere-Stratosphere-Troposphere) radar in Gadanki (Rao et al., 1995) has been used to characterize turbulence and gravity waves in the UTLS (Satheesan & Krishna Murthy, 2002) and their link with convection (Dutta et al., 2009; Shankar Das et al., 2010). Several studies have used the Equatorial Atmosphere Radar (EAR) from Koto Tabang, Sumatra, Indonesia (Dhaka et al., 2003, 2006). Most often, however, previous works on tropical winds from radar measurements focused on the horizontal wind component (Li et al., 2012), on investigating low frequency inertia gravity waves (Das et al., 2012; Kottayil et al., 2018) or on estimating gravity wave momentum fluxes (Dutta et al., 2009; Shankar Das et al., 2010). The time resolution used for those purposes is typically lower than required to fully resolve vertical motions. The study of w from radars has also often suffered from limited measurements at high frequency or a large fraction of missing data (e.g., due to a lack of radar echo).

In this paper, we present a new vertical wind dataset and demonstrate its quality and value for investigating tropical UTLS dynamics. The measurements were obtained from the recently built Advanced Center for Atmospheric Radar Research (ACARR) radar in Cochin, India which for the first time has been operated at high frequency (sampling cycle of 44 s), allowing precise characterization of fast atmospheric dynamics. The article is organized as follows. The radar data and w retrieval are described in Sect. 2, along with the external datasets used. Section 3 investigates the typical variability of w profiles and their climatological evolution over 5 months Section 4 discusses potential dynamical processes at play, examining the possibility of trapped waves and investigating the connection between vertical wind variability and (remote) convection. Conclusions are provided in Sect. 5.

2. Data and Methodology

2.1. Radar Data

Wind profiler radars estimate ambient-air vertical motion from the Doppler shift of back-scattered electromagnetic signals. Bragg scattering is the basic mechanism for radar echoes, although other scattering mechanisms such as non-turbulent scattering (Fresnel scattering) or scattering from anisotropic turbulence may also contribute to radar back scattering (Allen & Vincent, 1995; Doviak & Zrnic, 1984; Fukao & Hamazu, 2014; Minamihara et al., 2018; Yamamoto et al., 2003). The 205 MHz Stratosphere-Troposphere (ST) wind profiler radar at ACARR, Cochin University of Science and Technology, Cochin (10.04°N, 76.33°E), Kerala is an active phased array radar with 619 antenna elements and a diameter of approximately 27 m. It can probe an altitude range of 315 m to 20 km and can provide accurate three-dimensional wind components. The electronic beam steering capability of the radar allows for three-dimensional views of the atmosphere. Technical details and validation of a prototype 205 MHz radar wind profiler can be found in Kottayil et al. (2016) and Samson et al. (2016), and an assessment of this particular radar is provided in Mohanakumar et al. (2017). For the present study, the radar was operated in zenith mode and the w measurements were generated every 44 s continuously for 4 hr (12:00–16:00 local time, i.e. 06:30–10:30 UTC). The corresponding radar parameters are provided in the supplement, Table S1 in Supporting Information S1. In total, 63 days of w data gathered between 14 December 2022 and 11 April 2023 are used in this study.

The received signals, that is, in-phase and quadrature-phase signals, were archived for a number $n = 256$ of pulses, and a coherent integration was applied to improve the signal-to-noise ratio. This process was repeated to generate a time series of in phase and quadrature-phase signals for Fast Fourier Transform analysis, from which radar Doppler power spectra are created. To avoid contamination from interferences by stationary targets at ground level (non-moving objects like trees and artificial structures), the points corresponding to zero Doppler shift were replaced by interpolating the Doppler signal from adjacent points.

Vertical wind is then determined from the Doppler power spectrum at each altitude by identifying the Doppler shift at which the returned signal reaches its maximum value and converting it to the corresponding wind speed. This method performs well when the signal-to-noise ratio (SNR) is high and the signal peak clearly stands out; however, at altitudes where the received power is low, unrealistic Doppler shift values are sometimes picked. This is seen in Figures 1b and 1c where most sharp black peaks correspond to regions of low SNR; to exclude those points, we filter out measurements with received power lower than −165 dBm (the sensitivity threshold of the radar). The Doppler spectrum also becomes unreliable during the passage of aircraft in the side lobes of the radar beam, which can be identified as large-magnitude echos moving rapidly (from one scan to the next) in both range and Doppler shift. This is illustrated in Figure 1c near 14 km by the horizontal line of elevated signal strength. In

10.1029/2024GL110366

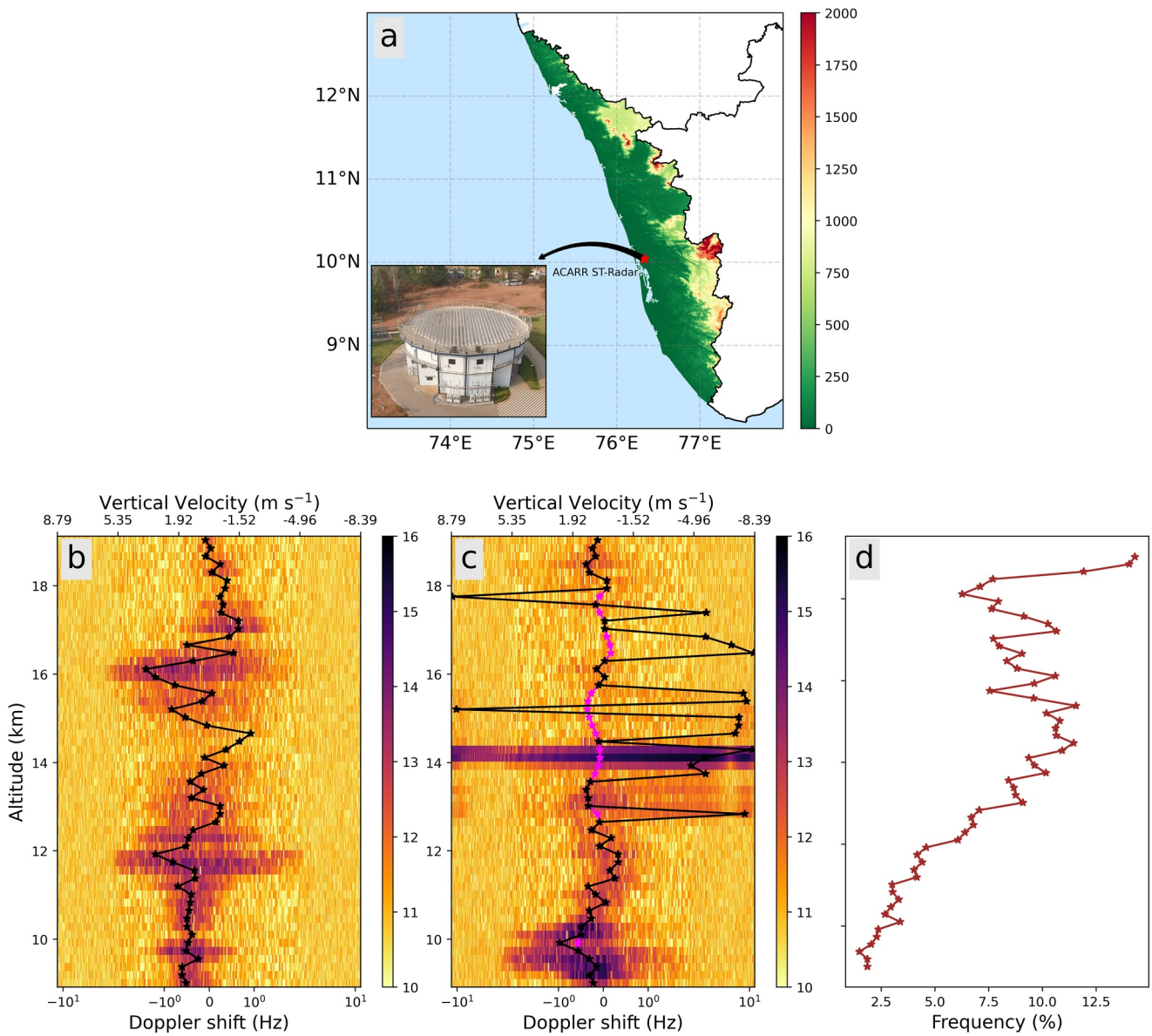

Figure 1. (a) Topographical map of Kerala (geometric altitude above sea level in meters) along with ACARR ST radar location (red star) and picture of the antenna array (b), (c) Doppler power spectra of vertical beam obtained on 31 January 2023, 13:13 local time and 2 March 2023, 8:17 local time, respectively. The unit of power is in dB, which is arbitrary. (d) Fraction of missing data (detected outliers) as a function of altitude during the measurement period.

order to remove outliers, w values thrice as large as and larger than the scaled median absolute deviations (MAD) are flagged as outliers and replaced using cubic spline interpolation in altitude. The magenta asterisk in the figure represents the interpolated values. For the sake of the spectral analysis of w time series, all flagged outliers are replaced using linear interpolation in time. It can also be seen that the Doppler width varies with altitude due to different broadening factors such as non-zero mean wind, wind shear, turbulence, etc (Nastrom, 1997, and references therein).

2.2. Ancillary Data Sets

Profiles of horizontal wind and potential temperature from the European Center for Medium-Range Weather Forecasts (ECMWF) ERA5 reanalysis on model levels (Hersbach et al., 2020) coincident with radar observations as well as Infrared (IR) brightness temperature (Tb) data in the 11 μm atmospheric window channel (GPM_MERGEIR) (Janowiak et al., 2017) have been used in this study to provide context for w observations.

GPM_MERGEIR is available at about 4 km spatial resolution and half an hour temporal resolution. The IR Tb is employed as a proxy for convection (Kottayil et al., 2021). A validation study by Sivan et al. (2021) shows that horizontal wind profiles from ERA5 match well with radar data within the UTLS.

3. Results

3.1. Selected Case Studies

Time-altitude sections of w on 16 December 2022 and 31 January 2023 are depicted in Figures 2b and 2d. These two dates were subjectively selected as representative of an active (16 December) and a quiet day (31 January). Indeed, while in both cases the typical amplitude of observed vertical wind fluctuations is of the order of 0.5 ms^{-1}, on 16 December, the upper part of the profile (above 14 km) typically exhibits larger values (∼1 m/s). The time-altitude patterns of the fluctuations are also qualitatively distinct between the 2 days. A common feature is the presence of vertical stripes, that is, vertically homogeneous w fluctuations a few (∼3) kilometers deep, evident in the upper part (14–19 km) of the profiles. These stripes, which have periods of a few minutes, mostly occur above the WMO tropopause. They are a common feature in our observations at Cochin, but have not been presented in published data from the MST Radar at the tropical Indian site of Gadanki (e.g., Dutta et al., 2009; Ravi Kiran et al., 2022). Lower down in the profile, in the troposphere (below 14 km), vertical wind fluctuations generally appear to have longer periods (tens of minutes). On 16 December 2022 in particular, there is a clear contrast between the dynamics of the different layers. Large (± 0.5–1 m s^{-1}), intermittent bursts of quasi-monochromatic oscillations with vertically orientated phase lines and period of about 4 min (fine stripes, e.g., around 14:00 or 15:30 Local time) dominate the signal in the upper troposphere-lower stratosphere (around 17 km) whereas long-period updrafts (a few hours long) are prominent at the bottom of the profiles. We also note an abrupt time shift in time of the phase lines of otherwise vertically coherent structures, for instance around 13:45 local time at 14.5 km.

To characterize the time scales present, the frequency power spectral densities (PSDs) of w are shown in Figure 2 (panels e–g) for the altitudes 10, 14 and 18 km. PSDs are estimated for both dates as the average of periodograms computed using Welch's method over 90 min windows with 30 min overlaps. They generally reveal two distinct frequency ranges: on the low-frequency side, the spectra remain rather flat until they drop more or less sharply around 1.5×10^{-3} Hz at 14 km and $3 - 4 \times 10^{-3}$ Hz at 18 km. Beyond these frequencies, they exhibit a steeper spectral slope. The transition between the two ranges may feature a prominent peak (at 18 km on 16 December 2022), show an abrupt change of slope (without a peak, e.g. at 10 km on 31 January), or be hardly distinguishable. It is tempting to identify the slope transition and the hump as the Brunt-Väisälä (B-V) frequency (indicated by the vertical lines in Figures 2e–2g). This assumption was made in previous analyses of vertical wind measurements from tropical radar sites (Revathy et al., 1996; Satheesan & Krishna Murthy, 2002); it appeared rooted in theory, which predicts a change of dynamical regime between gravity waves and inertial range turbulence near the B-V frequency (Fritts & Alexander, 2003). Above this frequency, freely propagating gravity waves are not supported (Nappo, 2012). Without disputing this interpretation in a statistical sense, our new observations challenge its systematic validity for individual vertical wind observations, as seen for instance at 14 km at which the hump is significantly shifted from ERA5 BVF. A more thorough geophysical interpretation of the different patterns observed in w will be provided in Sect. 4.

3.2. UTLS Vertical Wind Variance Over the Season

To quantify the variability of vertical wind over the whole measurement campaign, the altitude-time section of daily w variance $\left(\sigma_w^2\right)$, computed each day over the 4 hr period of observations, is shown in Figure 3a. Significant day-to-day variability in σ_w^2 is observed spanning the entire altitude range (10–19 km altitude), with values on active days in the range of 0.13–0.25 $m^2\ s^{-2}$, about fourfold than quiet days (0–0.06 $m^2\ s^{-2}$). Two distinct periods of enhanced σ_w^2 are visible in the figure (December 15-January 3 and January 22-Feburary 8). While these enhancements occur over the whole profile, they appear larger in the bottom part (10–15 km) than above.

Day-to-day variability in σ_w^2 is not unexpected. Previous studies have reported an abnormal increase of σ_w^2 in the UTLS related to the presence of deep convection in the immediate vicinity of the radar facility. Using MST radar observations, Hansen et al. (2002) found an increase of ${\sigma^2}_w$ to 0.6 $m^2\ s^{-2}$ at 10–12 km on thunderstorm days, while Dutta et al. (2009) observed ${\sigma^2}_w$ reaching up to three $m^2\ s^{-2}$ in the 10–15 km altitude range during deep convection. The potential link between deep convection and the variability in σ_w^2 will be further examined in Sect. 4.3.

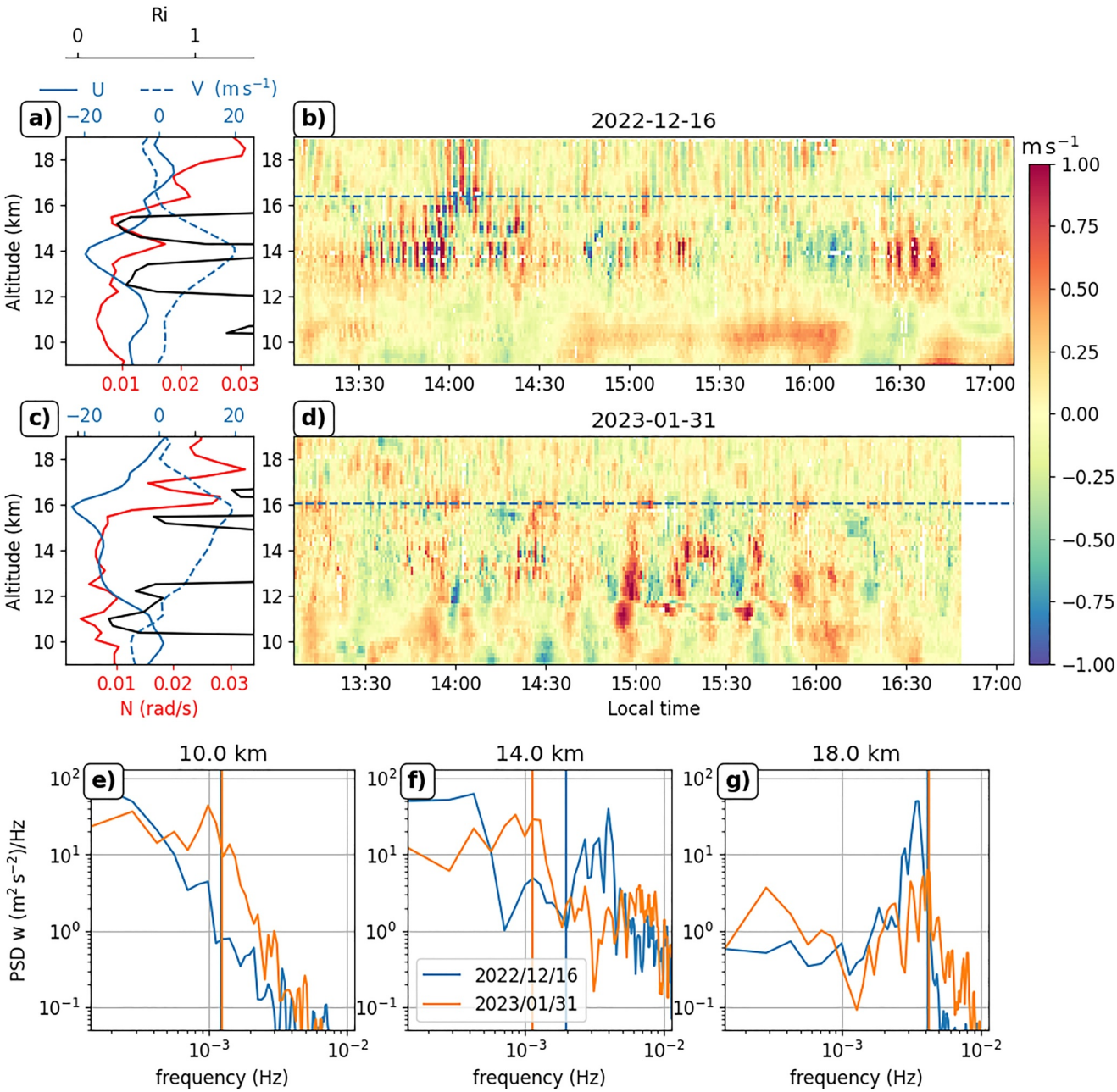

Figure 2. (a), (c) Altitude profiles of zonal (U) and meridional (V) winds, Brunt-Väisälä frequency and gradient Richardson number obtained from ERA5 for the period of 12:00 - 17:00 LT on 16 December 2022 and 31 January 2023 (b), (d) The time-altitude slices of *w* measured by the radar on 16 December 2022 and 31 January 2023. In panels (b), (d), the dashed horizontal blue line corresponds to the mean lapse rate tropopause altitude according to ERA5, following the World Meteorological Organization (WMO) definition (e, f, g) Corresponding periodograms of *w* at 10, 14 and 18 km altitude. Vertical lines represent B-V frequency for the corresponding dates (on panels e and g, the B-V for the two dates almost coincide).

4. Discussion

4.1. Evidence for Kelvin-Helmholtz Billows

A primary interpretation for alternating upward and downward motions would be billows associated with the development of a Kelvin-Helmholtz (K-H) instability (e.g., Luce et al., 2010; Minamihara et al., 2023). This is the most likely explanation for the 1 m/s *w* oscillations observed on 16 December around 13:45 local time between 13 and 15.5 km. A zoomed-in view of this pattern is provided in Figure 4, which highlights several features

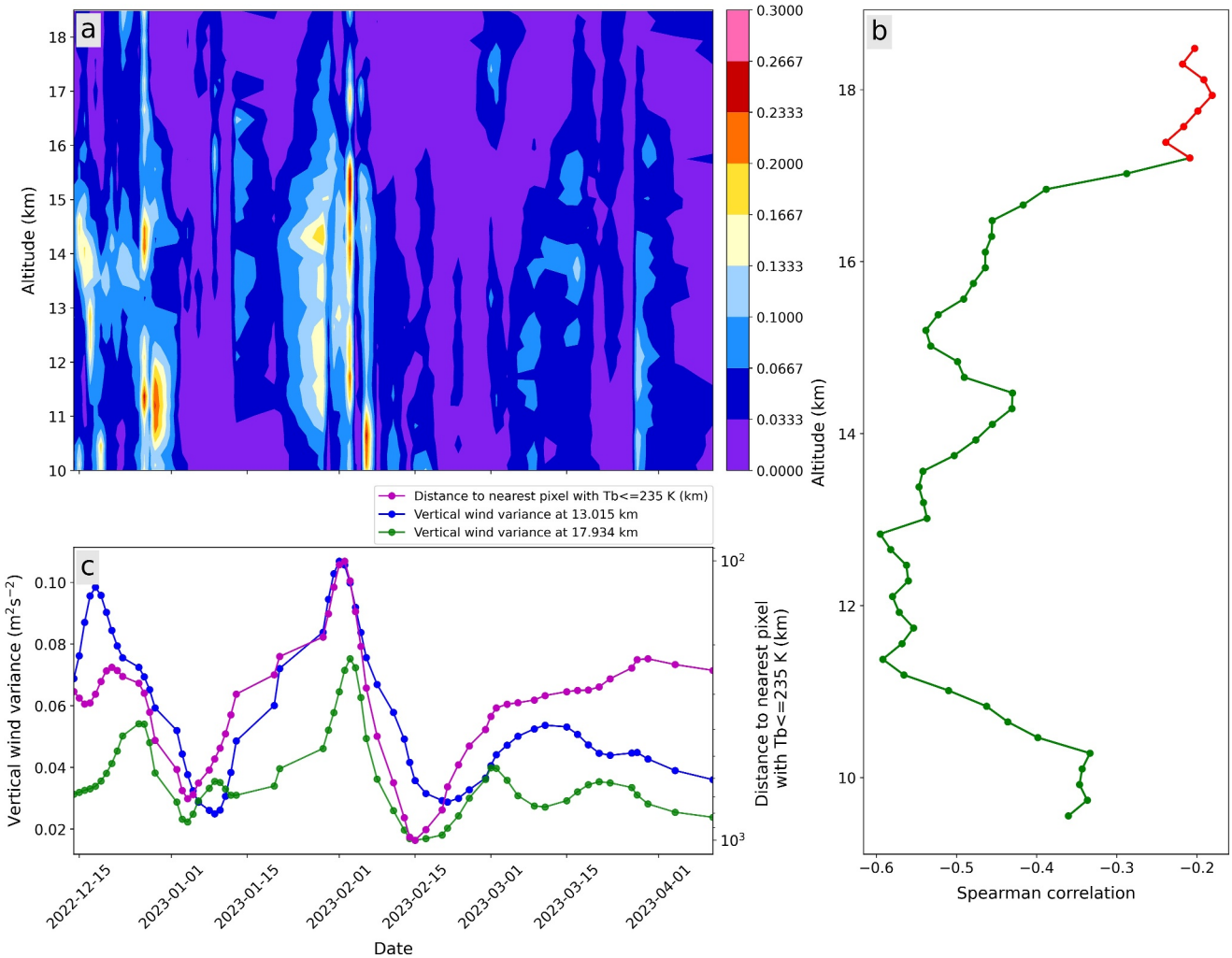

Figure 3. (a) Altitude-time section of w variance, σ_w^2 (b) Spearman correlation between daily σ_w^2 and distance to 11μm-brightness temperature at or lower than 235 K from the radar location. Green dots indicate significant correlation at the 95% p-value according to a Student t-test. (c) Time series of σ_w^2 at 13 and 17.9 km and the distance between the radar location and the nearest geostationary pixel with window (11 μm)-brightness temperature lower than 235 (K).

supporting the K-H interpretation. First, we note that the w vertical columns exhibit an abrupt phase shift of about one quarter phase around 14.5 km (Figure 4a). The radar echo power have a maximum near the w phase shift and a similar shape and phase relationship with w as reported for K-H braids by for example, Chapman and Browning (1997); Luce et al. (2010); Minamihara et al. (2023). Finally, the ERA5 indicates significant shear and a gradient Richardson number approaching the 0.25 threshold for K-H instability in that altitude range. Using the ERA5 mean wind over the 2.5 km deep layer occupied by the billows ($U \sim 20$ m/s) and assuming they are solely Doppler-shifted by the background flow, their 4 min apparent period translates into a horizontal wavelength of 4,800 m, which is again consistent with previous observations at other locations.

The K-H interpretation can however be ruled out for the stripes above 16 km, if we examine the same criterions: there is no tilt in the w columns; mean wind is weak in that altitude range (<5 m s^{-1}, Figure 2a), such that high-frequency w oscillations cannot arise only from Doppler shift by the mean wind; ERA5 Richardson numbers well above 0.25. The different geophysical phenomenon behind this feature is investigated in the next subsection.

4.2. Evidence for Trapped Waves

Above 16 km, the combination of coherent vertical stripes in time-altitude curtain and the hump near the B-V frequency in w spectra in a layer of low background wind (i.e., where ground-based and intrinsic frequency

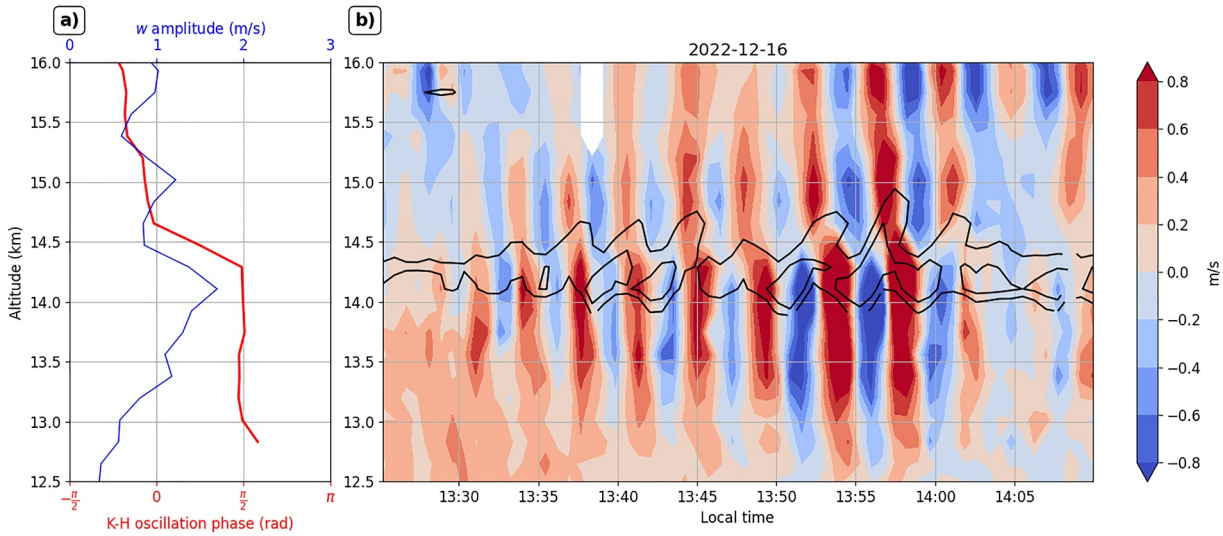

Figure 4. (a) Amplitude and phase (arbitrary reference) of the K-H billows in panel (b). (b) Detailed time-altitude section of w (colors) (zoomed-in version of Figure 2b) and radar echo power (black contours corresponding to 61 and 64 dB) highlighting their structure.

are equal) is suggestive of trapped or ducted high-frequency gravity waves (Nappo, 2012). The observed structures are reminiscent of horizontal distance-altitude vertical curtains observed in mountainous areas with an airborne lidar by Gisinger et al. (2020); Witschas et al. (2023), which the authors also interpreted as trapped waves.

In the framework of linear theory, the existence of vertically trapped gravity waves can be investigated using profiles of "squared vertical wavenumber" $m^2(z)$ (e.g., Nappo, 2012). Ignoring vertical shear of the horizontal wind, the dispersion relation reads (e.g., Fritts & Alexander, 2003):

$$m^2 = \left(k^2 + l^2\right)\left(\frac{N^2}{\hat{\omega}^2} - 1\right) - \frac{1}{4H^2} = \frac{N^2}{(U_k - c)^2} - \left(k^2 + l^2\right) - \frac{1}{4H^2} \tag{1}$$

where (k,l) is the horizontal wave number vector, $N(z)$ the B-V frequency and $\hat{\omega} = \omega - k\,U - l\,V$ the intrinsic wave frequency, (U,V) the horizontal wind vector, U_k its projection along the direction of wave propagation and $H \simeq 7$ km the density scale height. Vertically trapped waves occur in the presence of a compact isolated layer with $m^2(z;k,l,\omega) \geq 0$ (vertically propagating wave) sandwiched between layers of negative m^2 (i.e., m imaginary, corresponding to an evanescent wave whose amplitude decays exponentially on the vertical). This may occur through a combination of changes in N and $\hat{\omega}$ due to Doppler shift by the mean wind (i.e., the $k\,U + l\,V$ term).

While a detailed analysis is beyond the scope of the paper, we note that the increase of N across the tropopause combined with the changes in the wind magnitude and direction are favorable conditions for wave ducting. Indeed, according to Equation 1, m^2 decreases when N^2 is small and/or $(U_k - c)$ is large such that the waves tend to become external (i.e., $m^2 < 0$) in a height range with small N^2 and/or strong horizontal winds. Assuming small ground-based phase speed $c \ll |U_k|$, necessary conditions for the presence of trapped waves are given by the profile Scorer parameter $l^2(z) = N^2/\left(U^2 + V^2\right)$ (Nappo, 2012), which exhibits a local maximum near the tropopause on December 22, indicating favorable conditions for ducting and is shown in Figure 5.

A further argument in favor of wave trapping is the weak background wind (Figure 2a) in the altitude range of the quasi-monochromatic wave packets (16–19 km), meaning that intrinsic and ground-base wave frequency are nearly equal $\hat{\omega} \simeq \omega \simeq N$ (Figure 2g). Together with the quasi-vertical phase lines (i.e., $m^2/\omega^2 \to 0$), the observation $\hat{\omega} \simeq N$ suggests at least nearly trapped waves, in agreement with the dispersion relation (Equation 1).

Trapped waves were first described in the specific case of orographic flows and mountain lee waves (see, e.g., Scorer, 1949; Ralph et al., 1997) and have recently been studied in high-resolution geostationary satellite imagery (Stephan, 2020) or airborne Doppler-wind lidar w profiles (Gisinger et al., 2020). However, the vertical structure

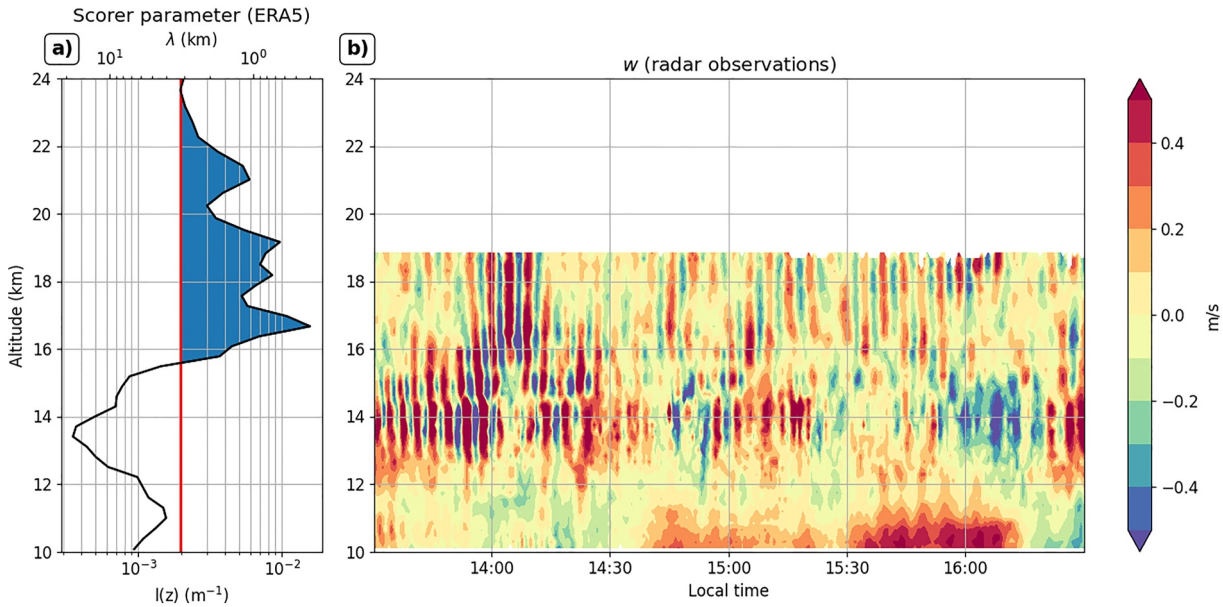

Figure 5. (a) Profile of the Scorer parameter $l(z) = \sqrt{N^2/(U^2 + V^2)}$ during the measurement period on 16 December 2022 according to ERA5 and (b) detailed time-altitude section of w (colors) (zoomed-in version of Figure 2b).

of the fluctuations could not be resolved in Stephan (2020), while Gisinger et al. (2020) investigated extra-tropical data. To our knowledge, w observations from the ACARR radar provide the clearest evidence so far of trapped wave occurrence and structure in the tropical UTLS. Li et al. (2012) interpreted observations from the Jicamarca radar as trapped waves, but their data consisted of horizontal wind measurements. An enhancement of vertical wind variability at intrinsic frequencies close to the B-V frequency, which would correspond to trapped waves, was noted in superpressure balloon observations near the tropopause by Podglajen et al. (2016) but with the caveat of possible measurement artifacts. In considering the possibility that the time-altitude stripes in w from radar are indeed trapped gravity waves, it is worth noting that they are a common feature visible in a large fraction (30%–50%) of the observation days used in this study, with variable amplitude. A possible factor influencing w variability is now discussed.

4.3. Relationship Between Vertical Wind Variability and Convection

Tropospheric deep convection can directly affect w variability, and is assumed to be a major source of tropical gravity waves (e.g., Beres et al., 2004), including trapped waves (Alexander et al., 2006). This is supported by observational (e.g., Alexander & Pfister, 1995; Corcos et al., 2021; Kottayil et al., 2018) and modeling (e.g., Köhler et al., 2023) studies of tropical gravity waves. The convective influence on gravity waves is not only local, but can be observed hundreds of kilometers away from the storm through lateral propagation (Corcos et al., 2021). Is convective variability modulating the pattern observed in $\sigma^2{}_w$ time series (Figure 3a) ? To answer this question, we have analyzed the distance between the radar location and the nearest pixel with 11 μm-brightness temperature lower than 235 K. Such low brightness temperature in the window channel indicates the presence of cold-top convective clouds (e.g., Kottayil et al., 2021).

The profile of Spearman (rank) correlation coefficient between $\sigma^2{}_w(z)$ and the distance to geostationary pixels with 11 μm-brightness temperature at and below 235 K is shown in Figure 3b. Throughout the profile, the anticorrelation between $\sigma^2{}_w$ and 11 μm-Tb appears significant. This anticorrelation is largest between 11 and 15 km (~ -0.55) and smaller (yet generally significant) correlations are observed above 17 km (~ 0.25) and below 11 km (~ -0.40). To further examining the link between convection and $\sigma^2{}_w$, the evolution of $\sigma^2{}_w$ at two representative height levels is depicted in Figure 3c along with distance to 11 μm-Tb at 235 K. The variance of w, $\sigma^2{}_w$, increases as the distance from the nearest deep convection decreases and vice versa.

5. Conclusions

This study aimed at investigating the variability of vertical wind (w) in the tropical UTLS from unprecedented high-frequency (periods shorter than 2 min) measurements obtained from the ACARR radar in Cochin, India. Our analysis suggested the high quality of ACARR w observations and their suitability to detect geophysical signatures.

Salient features in this new dataset include observations of K-H billows and frequent detection of high-frequency gravity waves, which we argue are trapped (or ducted) near the tropopause. To our knowledge, ACARR measurements are the most conclusive observations of trapped gravity waves in the tropical UTLS available at the time of writing. Those waves may play a significant role in shaping the variability of vertical wind near the tropopause. The impact of convection on w variance at the UTLS is also investigated. Low brightness temperature in the atmospheric window channel (i.e., convective activity) is well correlated with the velocity variance, in agreement with theoretical expectations and previous observational studies.

Future research should focus on identifying the generation processes of the observed trapped waves, assess their variability and contribution to w fluctuations, as well as explore possible implications for chemical or microphysical processes, such as ice nucleation (e.g., Dinh et al., 2016; Jensen et al., 2016).

Data Availability Statement

The vertical velocity data used in this study can be accessed from https://doi.org/10.5281/zenodo.10361753 (Kottayil, 2023).

Acknowledgments
This research was supported by the Indo-French Centre for the Promotion of Advanced Research (IFCPAR/CEFIPRA) project no 6707–2 (Variability of the upper-level asian monsoon anticyclone and mechanisms of its coupling with tropospheric monsoon convection) and the French Agence Nationale de la Recherche (ANR) under Grant 21-CE01-0016-01 (TuRTLES). Ministry of Earth Sciences (MoES), Government of India for the sustenance of the ACARR radar Facility is gratefully acknowledged.

References

Alexander, M. J., & Pfister, L. (1995). Gravity wave momentum flux in the lower stratosphere over convection. *Geophysical Research Letters*, *22*(15), 2029–2032. https://doi.org/10.1029/95GL01984

Alexander, M. J., Richter, J. H., & Sutherland, B. R. (2006). Generation and trapping of gravity waves from convection with comparison to parameterization. *Journal of the Atmospheric Sciences*, *63*(11), 2963–2977. https://doi.org/10.1175/JAS3792.1

Allen, S. J., & Vincent, R. A. (1995). Gravity wave activity in the lower atmosphere: Seasonal and latitudinal variations. *Journal of Geophysical Research*, *100*(D1), 1327–1350. Retrieved from https://doi.org/10.1029/94JD02688

Atlas, R., & Bretherton, C. S. (2023). Aircraft observations of gravity wave activity and turbulence in the tropical tropopause layer: Prevalence, influence on cirrus clouds, and comparison with global storm-resolving models. *Atmospheric Chemistry and Physics*, *23*(7), 4009–4030. https://doi.org/10.5194/acp-23-4009-2023

Bacmeister, J. T., Eckermann, S. D., Newman, P. A., Lait, L., Chan, K. R., Loewenstein, M., et al. (1996). Stratospheric horizontal wavenumber spectra of winds, potential temperature, and atmospheric tracers observed by high-altitude aircraft. *Journal of Geophysical Research*, *101*(D5), 9441–9470. https://doi.org/10.1029/95JD03835

Beres, J. H., Alexander, M. J., & Holton, J. R. (2004). A method of specifying the gravity wave spectrum above convection based on latent heating properties and background wind. *Journal of the Atmospheric Sciences*, *61*(3), 324–337. https://doi.org/10.1175/1520-0469(2004)061⟨0324:AMOSTG⟩2.0.CO;2

Chapman, D., & Browning, K. A. (1997). Radar observations of wind-shear splitting within evolving atmospheric kelvin-helmholtz billows. *Quarterly Journal of the Royal Meteorological Society*, *123*(541), 1433–1439. https://doi.org/10.1002/qj.49712354114

Corcos, M., Hertzog, A., Plougonven, R., & Podglajen, A. (2021). Observation of gravity waves at the tropical tropopause using superpressure balloons. *Journal of Geophysical Research: Atmospheres*, *126*(15), e2021JD035165. https://doi.org/10.1029/2021JD035165

Das, S. S., Uma, K. N., & Das, S. K. (2012). MST radar observations of short-period gravity wave during overhead tropical cyclone. *Radio Science*, *47*(2), RS2019. https://doi.org/10.1029/2011RS004840

Dauhut, T., Chaboureau, J.-P., Haynes, P. H., & Lane, T. P. (2018). The mechanisms leading to a stratospheric hydration by overshooting convection. *Journal of the Atmospheric Sciences*, *75*(12), 4383–4398. https://doi.org/10.1175/JAS-D-18-0176.1

Dhaka, S. K., Takahashi, M., Shibagaki, Y., Yamanaka, M. D., & Fukao, S. (2003). Gravity wave generation in the lower stratosphere due to passage of the typhoon 9426 (orchid) observed by the mu radar at shigaraki (34.85°n, 136.10°e). *Journal of Geophysical Research*, *108*(D19). Retrieved from https://doi.org/10.1029/2003JD003489

Dhaka, S. K., Yamamoto, M. K., Shibagaki, Y., Hashiguchi, H., Fukao, S., & Chun, H. Y. (2006). Equatorial Atmosphere Radar observations of short vertical wavelength gravity waves in the upper troposphere and lower stratosphere region induced by localized convection. *Geophysical Research Letters*, *33*(19), L19805. https://doi.org/10.1029/2006GL027026

Dinh, T., Podglajen, A., Hertzog, A., Legras, B., & Plougonven, R. (2016). Effect of gravity wave temperature fluctuations on homogeneous ice nucleation in the tropical tropopause layer. *Atmospheric Chemistry and Physics*, *16*(1), 35–46. https://doi.org/10.5194/acp-16-35-2016

Doviak, R. J., & Zrnic, D. S. (1984). Reflection and scatter formula for anisotropically turbulent air. *Radio Science*, *19*(1), 325–336. https://doi.org/10.1029/RS019i001p00325

Dutta, G., Ajay Kumar, M. C., Vinay Kumar, P., Venkat Ratnam, M., Chandrashekar, M., Shibagaki, Y., et al. (2009). Characteristics of high-frequency gravity waves generated by tropical deep convection: Case studies. *Journal of Geophysical Research (Atmospheres)*, *114*(D18), D18109. https://doi.org/10.1029/2008JD011332

Fritts, D. C., & Alexander, M. J. (2003). Gravity wave dynamics and effects in the middle atmosphere. *Reviews of Geophysics*, *41*(1). https://doi.org/10.1029/2001RG000106

Fujiwara, M., Yamamoto, M. K., Hashiguchi, H., Horinouchi, T., & Fukao, S. (2003). Turbulence at the tropopause due to breaking Kelvin waves observed by the Equatorial Atmosphere Radar. *Geophysical Research Letters*, *30*(4). Retrieved 2024-01-10, from. https://doi.org/10.1029/2002GL016278

Fukao, S., & Hamazu, K. (2014). *Radar for meteorological and atmospheric observations*. Springer.

Gisinger, S., Wagner, J., & Witschas, B. (2020). Airborne measurements and large-eddy simulations of small-scale gravity waves at the tropopause inversion layer over Scandinavia. *Atmospheric Chemistry and Physics*, *20*(16), 10091–10109. https://doi.org/10.5194/acp-20-10091-2020

Grant, L. D., van den Heever, S. C., Haddad, Z. S., Bukowski, J., Marinescu, P. J., Storer, R. L., et al. (2022). A linear relationship between vertical velocity and condensation processes in deep convection. *Journal of the Atmospheric Sciences*, *79*(2), 449–466. Retrieved from https://doi.org/10.1175/JAS-D-21-0035.1

Hansen, A. R., Nastrom, G. D., Otkin, J. A., & Eaton, F. D. (2002). Mst radar observations of gravity waves and turbulence near thunderstorms. *Journal of Applied Meteorology*, *41*(3), 298–305. Retrieved from https://doi.org/10.1175/1520-0450(2002)041⟨0298:MROOGW⟩2.0.CO;2

Hersbach, H., Bell, B., Berrisford, P., Hirahara, S., Horányi, A., Muñoz-Sabater, J., et al. (2020). The era5 global reanalysis. *Quarterly Journal of the Royal Meteorological Society*, *146*(730), 1999–2049. Retrieved from https://doi.org/10.1002/qj.3803

Hertzog, A., & Vial, F. (2001). A study of the dynamics of the equatorial lower stratosphere by use of ultra-long-duration balloons: 2. Gravity waves. *Journal of Geophysical Research*, *106*(D19), 22745–22761. Retrieved from https://doi.org/10.1029/2000JD000242

Janowiak, J., Joyce, B., & Xie, P. (2017). In A. Savtchenko (Ed.), *NCEP/CPC L3 half hourly 4km global (60S - 60N) merged IR V1*. Goddard Earth Sciences Data and Information Services Center (GES DISC). Accessed 2023.

Jensen, E. J., Ueyama, R., Pfister, L., Bui, T. V., Alexander, M. J., Podglajen, A., et al. (2016). High-frequency gravity waves and homogeneous ice nucleation in tropical tropopause layer cirrus. *Geophysical Research Letters*, *43*(12), 6629–6635. https://doi.org/10.1002/2016GL069426

Köhler, L., Green, B., & Stephan, C. C. (2023). Comparing Loon superpressure balloon observations of gravity waves in the tropics with global storm-resolving models. *Journal of Geophysical Research: Atmospheres*, *128*(15), e2023JD038549. n/a(n/a). https://doi.org/10.1029/2023JD038549

Kottayil, A. (2023). Radar high resolution vertical velocity. [Dataset]. https://doi.org/10.5281/zenodo.10361753. *zenedo*

Kottayil, A., Mohanakumar, K., Samson, T., Rebello, R., Manoj, M. G., Varadarajan, R., et al. (2016). Validation of 205 mhz wind profiler radar located at cochin, India, using radiosonde wind measurements. *Radio Science*, *51*(3), 106–117. https://doi.org/10.1002/2015RS005836

Kottayil, A., Satheesan, K., John, V. O., & Antony, R. (2021). Diurnal variation of deep convective clouds over Indian monsoon region and its association with rainfall. *Atmospheric Research*, *255*, 105540. https://doi.org/10.1016/j.atmosres.2021.105540

Kottayil, A., Satheesan, K., Mohankumar, K., Chandran, S., & Samson, T. (2018). An investigation into the characteristics of inertia gravity waves in the upper troposphere/lower stratosphere using a 205 mhz wind profiling radar. *Remote Sensing Letters*, *9*(3), 284–293. https://doi.org/10.1080/2150704X.2017.1418991

Legras, B., & Bucci, S. (2020). Confinement of air in the Asian monsoon anticyclone and pathways of convective air to the stratosphere during the summer season. *Atmospheric Chemistry and Physics*, *20*(18), 11045–11064. https://doi.org/10.5194/acp-20-11045-2020

Li, Z., Naqvi, S., Gerrard, A. J., Chau, J. L., & Bhattacharya, Y. (2012). Initial MST radar observations of upper tropospheric-lower stratospheric duct-like structures over Jicamarca, Peru. *Atmospheric Chemistry and Physics*, *12*(22), 11085–11093. https://doi.org/10.5194/acp-12-11085-2012

Luce, H., Mega, T., Yamamoto, M. K., Yamamoto, M., Hashiguchi, H., Fukao, S., et al. (2010). Observations of Kelvin-Helmholtz instability at a cloud base with the middle and upper atmosphere (MU) and weather radars. *Journal of Geophysical Research*, *115*(D19). https://doi.org/10.1029/2009JD013519

Minamihara, Y., Sato, K., & Tsutsumi, M. (2023). Kelvin-Helmholtz billows in the troposphere and lower stratosphere detected by the PANSY radar at syowa station in the antarctic. *Journal of Geophysical Research: Atmospheres*, *128*(5), e2022JD036866. https://doi.org/10.1029/2022JD036866

Minamihara, Y., Sato, K., Tsutsumi, M., & Sato, T. (2018). Statistical characteristics of gravity waves with near-inertial frequencies in the antarctic troposphere and lower stratosphere observed by the PANSY radar. *Journal of Geophysical Research (Atmospheres)*, *123*(17), 8993–9010. https://doi.org/10.1029/2017JD028128

Mohanakumar, K., Kottayil, A., Anandan, V. K., Samson, T., Thomas, L., Satheesan, K., et al. (2017). Technical details of a novel wind profiler radar at 205 mhz. *Journal of Atmospheric and Oceanic Technology*, *34*(12), 2659–2671. https://doi.org/10.1175/JTECH-D-17-0051.1

Nappo, C. J. (2012). Ducted gravity waves. *An Introduction to Atmospheric Gravity Waves*, *102*, 87–116. Elsevier. https://doi.org/10.1016/B978-0-12-385223-6.00004-5

Nastrom, G. D. (1997). Doppler radar spectral width broadening due to beamwidth and wind shear. *Annales Geophysicae*, *15*(6), 786–796. Retrieved from https://doi.org/10.1007/s00585-997-0786-7

Pfister, L., Starr, W., Craig, R., Loewenstein, M., & Legg, M. (1986). Small-scale motions observed by aircraft in the tropical lower stratosphere: Evidence for mixing and its relationship to large-scale flows. *Journal of the Atmospheric Sciences*, *43*(24), 3210–3225. Retrieved from https://doi.org/10.1175/1520-0469(1986)043⟨3210:SSMOBA⟩2.0.CO;2

Podglajen, A., Bui, T. P., Dean-Day, J. M., Pfister, L., Jensen, E. J., Alexander, M. J., et al. (2017). Small-scale wind fluctuations in the tropical tropopause layer from aircraft measurements: Occurrence, nature, and impact on vertical mixing. *Journal of the Atmospheric Sciences*, *74*(11), 3847–3869. https://doi.org/10.1175/JAS-D-17-0010.1

Podglajen, A., Hertzog, A., Plougonven, R., & Legras, B. (2016). Lagrangian temperature and vertical velocity fluctuations due to gravity waves in the lower stratosphere. *Geophysical Research Letters*, *43*(7), 3543–3553. https://doi.org/10.1002/2016GL068148

Podglajen, A., Hertzog, A., Plougonven, R., & Legras, B. (2020). Lagrangian gravity wave spectra in the lower stratosphere of current (re)analyses. *Atmospheric Chemistry and Physics*, *20*(15), 9331–9350. https://doi.org/10.5194/acp-20-9331-2020

Ralph, F. M., Neiman, P. J., Keller, T. L., Levinson, D., & Fedor, L. (1997). Observations, simulations, and analysis of nonstationary trapped lee waves. *Journal of the Atmospheric Sciences*, *54*(10), 1308–1333. https://doi.org/10.1175/1520-0469(1997)054⟨1308:OSAAON⟩2.0.CO;2

Rao, P. B., Jain, A. R., Kishore, P., Balamuralidhar, P., Damle, S. H., & Viswanathan, G. (1995). Indian MST radar 1. System description and sample vector wind measurements in ST mode. *Radio Science*, *30*(4), 1125–1138. https://doi.org/10.1029/95RS00787

Ravi Kiran, V., Venkat Ratnam, M., Fujiwara, M., Russchenberg, H., Wienhold, F. G., Madhavan, B. L., et al. (2022). Balloon-borne aerosol–cloud interaction studies (BACIS): Field campaigns to understand and quantify aerosol effects on clouds. *Atmospheric Measurement Techniques*, *15*(16), 4709–4734. https://doi.org/10.5194/amt-15-4709-2022

Revathy, K., Prabhakaran Nair, S. R., & Krisha Murthy, B. V. (1996). Deduction of temperature profile from MST radar observations of vertical wind. *Geophysical Research Letters*, *23*(3), 285–288. https://doi.org/10.1029/96GL00086

Samson, T. K., Kottayil, A., Manoj, M. G., Binoy Babu, B., Rakesh, V., Rebello, R., et al. (2016). Technical aspects of 205 MHz VHF mini wind profiler radar for tropospheric probing. *IEEE Geoscience and Remote Sensing Letters*, *13*(7), 1027–1031. https://doi.org/10.1109/LGRS.2016.2561965

Satheesan, K., & Krishna Murthy, B. V. (2002). Turbulence parameters in the tropical troposphere and lower stratosphere. *Journal of Geophysical Research*, *107*(D1), 4002. https://doi.org/10.1029/2000JD000146

Schumacher, C., Stevenson, S. N., & Williams, C. R. (2015). Vertical motions of the tropical convective cloud spectrum over Darwin, Australia. *Quarterly Journal of the Royal Meteorological Society*, *141*(691), 2277–2288. Retrieved from https://doi.org/10.1002/qj.2520

Schumann, U. (2019). The horizontal spectrum of vertical velocities near the tropopause from global to gravity wave scales. *Journal of the Atmospheric Sciences*, *76*(12), 3847–3862. https://doi.org/10.1175/JAS-D-19-0160.1

Scorer, R. S. (1949). Theory of waves in the lee of mountains. *Quarterly Journal of the Royal Meteorological Society*, *75*(323), 41–56. https://doi.org/10.1002/qj.49707532308

Scott, S. G., Bui, T. P., Chan, K. R., & Bowen, S. W. (1990). The meteorological measurement system on the NASA ER-2 aircraft. *Journal of Atmospheric and Oceanic Technology*, *7*(4), 525–540. https://doi.org/10.1175/1520-0426(1990)007⟨0525:TMMSOT⟩2.0.CO;2

Shankar Das, S., Kishore Kumar, K., & Uma, K. N. (2010). MST radar investigation on inertia-gravity waves associated with tropical depression in the upper troposphere and lower stratosphere over Gadanki (13.5°N, 79.2°E). *Journal of Atmospheric and Solar-Terrestrial Physics*, *72*(16), 1184–1194. https://doi.org/10.1016/j.jastp.2010.07.016

Sivan, C., Kottayil, A., Legras, B., Bucci, S., Mohanakumar, K., & Satheesan, K. (2022). Tracing the convective sources of air at tropical tropopause during the active and break phases of Indian summer monsoon. *Climate Dynamics*, *59*(9–10), 2717–2734. https://doi.org/10.1007/s00382-022-06238-9

Sivan, C., Rakesh, V., Abhilash, S., & Mohanakumar, K. (2021). Evaluation of global reanalysis winds and high-resolution regional model outputs with the 205 MHz stratosphere-troposphere wind profiler radar observations. *Quarterly Journal of the Royal Meteorological Society*, *147*(737), 2562–2579. https://doi.org/10.1002/qj.4041

Stephan, C. C. (2020). Seasonal modulation of trapped gravity waves and their imprints on trade wind clouds. *Journal of the Atmospheric Sciences*, *77*(9), 2993–3009. https://doi.org/10.1175/JAS-D-19-0325.1

Uma, K. N., Das, S. S., Ratnam, M. V., & Suneeth, K. V. (2021). Assessment of vertical air motion among reanalyses and qualitative comparison with very-high-frequency radar measurements over two tropical stations. *Atmospheric Chemistry and Physics*, *21*(3), 2083–2103. https://doi.org/10.5194/acp-21-2083-2021

Wang, L., Alexander, M. J., Bui, T. B., & Mahoney, M. J. (2006). Small-scale gravity waves in er-2 mms/mtp wind and temperature measurements during crystal-face. *Atmospheric Chemistry and Physics*, *6*(4), 1091–1104. Retrieved from https://acp.copernicus.org/articles/6/1091/2006/doi:10.5194/acp-6-1091-2006

Witschas, B., Gisinger, S., Rahm, S., Dörnbrack, A., Fritts, D. C., & Rapp, M. (2023). Airborne coherent wind lidar measurements of the momentum flux profile from orographically induced gravity waves. *Atmospheric Measurement Techniques*, *16*(4), 1087–1101. https://doi.org/10.5194/amt-16-1087-2023

Yamamoto, M. K., Oyamatsu, M., Horinouchi, T., Hashiguchi, H., & Fukao, S. (2003). High time resolution determination of the tropical tropopause by the Equatorial Atmosphere Radar. *Geophysical Research Letters*, *30*(21), 2094. https://doi.org/10.1029/2003GL018072